Highly Dispersed Polyamide-11/Halloysite Nanocomposites: Thermal, Rheological, Optical, Dielectric, and Mechanical Properties

Kalappa Prashantha, Marie-France Lacrampe, Patricia Krawczak

Mines Douai, Department of Polymers and Composites Technology & Mechanical Engineering, F-59508 Douai Cedex, France
Correspondence to: K. Prashantha (E-mail: kalappa.prashantha@mines-douai.fr)

ABSTRACT: Bio-based polyamide 11 and natural halloysite nanotubes (HNTs) were used for the preparation of PA-11/HNT nanocomposites with varying nanotubes concentrations by melt extrusion using a masterbatch dilution process. The prepared nanocomposites were analyzed for microstructural changes, transparency, thermal stability, rheological behavior, dielectric, and mechanical properties. The HNT nanotubes are well dispersed in PA-11 matrix in the studied composition range as shown by microscopy and spectrophotometry. Interestingly, good halloysite dispersion in PA-11 matrix increases the tensile strength and Young modulus of PA-11 without sacrificing the ductility. Highly dispersed nanotubes also bring favorable changes in the thermal stability, dielectric, and rheological characteristics of PA-11. Additionally, glass transition temperature, crystallization temperature, and degree of crystallinity of the nanocomposites tend to increase with increase in nanotubes loading. Thus, PA-11 can become a tailor-made material with multifunctional characteristics, thanks to the addition of HNTs. © 2013 Wiley Periodicals, Inc. J. Appl. Polym. Sci. 130: 313–321, 2013

INTRODUCTION

There is a growing interest in the development of multifunctional polymers systems by incorporating low amounts of nanofillers.[1,2] Compounding and processing of such materials have to be carefully mastered, as the final properties of the obtained nanocomposites strongly depend on the nanofillers dispersion state and the microstructural changes locally induced upon nanoparticle addition. Polyamide matrices are often used to develop such nanocomposites. In particular, the literature extensively reported the numerous efforts produced to improve the thermomechanical, rheological, barrier, and flame retardancy properties of polyamide-66 by incorporating a small amount of nanofillers such as montmorillonite (MMT),[3–6] inorganic particles,[7,8] and carbon nanotubes (CNTs)[9–11] to produce high-performance polymeric nanocomposite materials.

In the family of polyamides, polyamide-11 (PA-11) is also a semi-crystalline engineering polyamide. This polymer may be fully biobased when synthesized using castor oil. Moreover, its structure may be tuned to render it piezoelectric. However, studies on the PA-11-based nanocomposites are very limited in the literature.[12] The electroactive behaviors such as piezoelectric, ferroelectric, and dielectric properties of biaxially oriented PA-11 films, with and without ceramic fillers have been exploited.[13–18] Fact of the matter is, inclusion of ceramic fillers

lowers the mechanical properties, increases the density and toxicity of final product, thereby limiting the application of PA-11. Nevertheless, recent literature suggests that the microstructure and ultimate properties of PA-11 can be modified by the addition of nanofillers such as MMTs or CNTs.[19–22] Unfortunately, the reported results appear to be contradictory. Liu et al.[19] mentioned a negligible enhancement in mechanical properties of PA-11 even at high organoclay loadings which was ascribed to incomplete exfoliation of nanoparticles. Mago et al.[21] reported a significant improvement in modulus and strength upon addition of CNTs and carbon nanofiber to PA-11, but decreased toughness.[21] Recently, Stoclet et al.[22] obtained exfoliated PA-11/clay nanocomposites by water-assisted extrusion process and observed significant enhancement in the mechanical properties and thermal stability.

Besides, halloysite nanotubes (HNTs) are two-layered aluminosilicate minerals, which are available in abundance in many locations around the world. It is chemically similar to kaolin, differing mainly in the morphology of crystals.[23] HNTs possess hollow nanotubular structure with large specific surface area. HNTs exhibit a high aspect ratio with nanotube length of 1–15 μm with inner and outer diameters of 15–100 and 40–120 nm, respectively.[23] Compared to CNTs, HNTs are naturally available, biocompatible, and much cheaper.[23] Moreover, HNTs have low density of hydroxyl functional groups when compared

to clays, which makes HNTs disperse in a polymer matrix better than CNTs or clays. Novel thermomechanical and chemical properties of HNTs have provided opportunity as low-cost and effective nanofillers for polymer matrix and hence have been incorporated into polymers.[24–27] Previous studies from our laboratory[28–30] and the reports from other researchers[31–33] indicate that incorporation of HNTs improves the thermomechanical properties of the nanocomposites. HNTs also provide strength increase without loss of ductility. Importantly, HNTs are biocompatible materials and their usage in drug delivery, bioreactors, and genes delivery applications is well established in the literature.[13–17]

As mentioned above, it is well known that the performance of nanocomposites depends on the dispersion state of nanofillers in the polymer matrix. Uniform dispersion of nanofillers in a polymer matrix is still a challenge. Previous studies from our laboratory proposed a masterbatch dilution technique as an effective means of dispersing nanofillers in thermoplastic matrices,[4,28–30,34] making it possible to achieve a better dispersion of fillers when compared to direct mixing methods.

Consequently, it makes sense to design polymer nanocomposites with multifunctional properties using naturally available HNTs and bio-based PA-11 and to compound such materials using a masterbatch dilution technique. Therefore, in this study, PA-11/HNT nanocomposites were prepared by melt-compounding via a masterbatch dilution process. Effect of HNTs on the morphology, thermal properties, rheological characteristics, dynamic mechanical behavior, and tensile properties of nanocomposites were investigated.

EXPERIMENTAL

Materials
HNTs used in this study have an average diameter of 80 nm, a length of about 1.2 μ, and a density of 2.5 g/cm^3 (Natural Nano, USA). Polyamide-11 (PA-11) is an injection grade (BMNO TLD, Rilsan®, Arkema). Before processing, PA-11 pellets and HNTs were dried under vacuum at 80°C for 8 h and 4 h, respectively, to remove moisture traces.

Compounding of Masterbatches
Masterbatch dilution technique was adopted to prepare nanocomposites containing the desired halloysite loading. Therefore, masterbatches containing 15 wt % of halloysites were prepared by adding HNTs in the melt zone of twin-screw extruder (Haake Polylab OS, Thermoscientific, USA) equipped with a screw of $D = 16$ mm diameter and $L/D = 40$ length to diameter ratio. Separate volumetric feeders were used for the HNTs and the PA-11. The temperature profile of the extruder was set at 220°C in the feed zone, sequentially at 225, 227, 230, and 232°C in the metering zone and 235°C at the die. The screw speed and feed rate were set at 60 rpm and 1000 g h^{-1}, respectively. Extruded material was cut into small pellets in a pelletizer (SGS 25-E4, Scheer, Germany). Masterbatch pellets were dried at 80°C in vacuum oven for overnight to remove residual water content for further utilization.

Processing of Nanocomposites
The prepared PA-11/HNT masterbatches were diluted to 2, 4, and 6 wt % HNT-filled nanocomposites by melt-compounding by mixing neat PA-11 granules with the masterbatch pellets in a single-screw extruder (Rheocord System 40, Haake Buchler Product, Germany) at a screw speed of 60 rpm. The temperatures setting from the hopper to the die was 225/230/235/240°C. Approximately, 2 kg of each formulation was produced using similar processing conditions. During melt extrusion, ventilation was kept on to remove trapped air in the compounds. Nanocomposites bearing 2, 4, and 6 wt % fillers in the PA-11 matrix were fabricated. Unfilled PA-11 pellets were also processed under the same conditions as a reference material. After pelletizing, the nanocomposites and PA-11 granules were dried for 5 h under vacuum at 80°C before injection molding.

Standard test specimens for tensile and dynamic mechanical analysis were molded using an electric injection-molding machine (KM80-160E, KraussMaffei, Germany). The temperature profile setting ranged from 225 to 235°C and the mold temperature was maintained at 25°C with water-cooling system. The holding pressure and screw rotation speed were 300 bar and 100 rpm, respectively, with a throughput of 50 cm^3 s^{-1}.

For rheological, dielectric, and UV–visible measurements, the nanocomposites were prepared by compression molding using a hydraulic press (Dolouets, France). Extruded PA-11 and its nanocomposite granules were placed between polytetrafluroethylene films and pressed between steel plates into 1-mm thick at 230°C during 2 min with a pressure of 100 bar and the samples were cooled to ambient temperature. All the materials were stored at 25°C and 50% relative humidity (RH) for 1 week before testing.

Scanning Electron Microscopy and Transmission Electron Microscopy
The fracture surfaces of the materials were observed by scanning electron microscopy (SEM) under high vacuum with a SEM instrument (S-4300SE/N, Hitachi, Japan) operating at 5 kV, the injection-molded cryofractured samples being previously coated with a thin gold layer.

Specimens for transmission electron microscopy (TEM) analysis were cut from bulk samples using a microtome (Reichert, Switzerland). Thin sections of approximately 90 nm in thickness were cut using an ultra-diamond knife. TEM images were obtained using a TEM instrument (LEO 922, Zeiss, Germany) with an acceleration voltage of 200 kV.

Optical Properties
The transparency of the materials was determined on film samples by means of a UV–visible spectrophotometer (Cary 500 Scan UV–vis spectrophotometer, USA). The percentage of transmittance between 200 and 800 nm was measured at five different locations of the samples.

Thermogravimetric Analysis
The thermal stability of the samples was measured with a thermogravimetric analyzer (TGA, Mettler, France). Sample masses ranging from 3 and 5 mg were heated from 25 to 600°C at a

heating rate of 20°C min^{-1} in a dry nitrogen atmosphere. The flow rate of nitrogen was 20 mL min^{-1}.

Differential Scanning Calorimetry

Thermal transitions of the materials were examined by differential scanning calorimetry (DSC 7 Perkin-Elmer, USA) under nitrogen flow (80 mL min^{-1}). Samples were crimple-sealed in aluminum crucibles and heated from 30 to 220°C at a heating rate of 10°C min^{-1} (first heating scan), equilibrated at 220°C for 5 min, cooled at 10°C min^{-1} to 30°C, equilibrated at 30°C for 5 min, and then heated again to 220°C at 10°C min^{-1} (second heating scan). The first heating scan was performed to eliminate the sample's thermal history. The crystallization temperature (T_c), melting temperature (T_m), crystallization enthalpy (ΔH_c), and melting enthalpy (ΔH_m) were determined. The degree of crystallanity (X_c) was calculated using eq. (1):

$$\chi_c = \frac{\Delta H_m}{\Delta H_m^0 (1 - w_t)} \times 100 \tag{1}$$

where ΔH_m is the melting enthalpy, ΔH_m^0 the melting enthalpy for 100% crystalline sample ($\Delta H_c^0 = 206$ J g^{-1}),[35] and "w_t" the filler weight fraction in the nanocomposites.

Dynamic Rheology

Oscillatory shear measurements were performed using an advanced rheometric expansion system (ARES, TA Instruments, Germany). The measurements were performed at 230°C using cone and plate geometry (diameter, 25 mm). The gap between the two plates was 0.4554 mm. Samples were equilibrated at 230°C for 3 min before testing. A strain sweep test was first performed to determine the linear viscoelastic region of the materials, and a shear strain of 0.6% was then chosen for all subsequent frequency sweep tests. The frequency was varied from 0.1 to 100 rad s^{-1}.

Dynamic Mechanical Analysis

The viscoelastic behavior was studied in tension by dynamic mechanical analysis (DMA + 150, MetraviB, France). Dynamic strain sweep was first performed to determine the linear viscoelastic range of the materials. The tests were then performed at a strain amplitude of 0.02% and a frequency of 1 Hz. Data were collected from −50 to 120°C at a scanning rate of 3°C min^{-1}. Rectangular DMA specimens (nominal dimensions, $4 \pm 0.2 \times 10 \pm 0.5 \times 30$ mm^3) were cut from injection-molded impact bar samples. Five specimens of each composition were tested at least.

Dielectric Properties Characterization

Dielectric characterization can provide information on the molecular dynamics of polymer systems, monitoring the relaxation processes. Moreover, the dielectric properties of nanohybrids are of technological interest because they represent the capability to store/dissipate energy under the application of an electric field. It is determined by the ability of a material to polarize in response to the applied field. Owing to its frequency dependence, the permittivity of a material is often represented by the complex permittivity ε^* and is defined as

$$\varepsilon^* = \varepsilon' - i\varepsilon'' \tag{2}$$

where ε' is the real part or dielectric constant and ε'' is the imaginary part of the dielectric permittivity. The dielectric constant for a polymer depends on the polarizability of its molecules. High molecular polarizability leads to high ε^*. As a heterogeneous system, a composite has also its dielectric properties influenced by interfacial polarization, that is, charge build up at the interfaces.

The dielectric characteristics of the materials were measured on film samples and calculated from capacitance measurements in the range of 50 Hz–1 MHz, by the use of an impedance bridge (LCR HP 4284A), in conjunction with the area of the aluminum electrodes. The accuracy of the dielectric measurement was confirmed by measuring the permittivity and tan δ of a standard polytetrafluoroethylene sample provided by the manufacturers. For each filler concentration, at least five samples were tested. All the measurements were performed at 25°C and 50% RH.

Tensile Testing

The mechanical properties were evaluated from injection-molded specimens. Tensile properties such as strength, modulus, and elongation at break were measured using a tensile machine (Model 1185, Instron, USA) at a crosshead rate of 10 mm min^{-1} at 25°C and 50% RH according to ISO 527 standard. At least five specimens of each composition were tested.

RESULTS AND DISCUSSION

Nanotubes Dispersion

SEM imaging reveals the homogeneous dispersion of HNTs in PA-11 matrix for all compositions (Figure 1). Nanocomposites containing 2, 4, and 6 wt % HNTs show individual nanotubes distributed throughout the matrix without any clusters even at higher (6 wt %) nanotube loading. In addition, no debonded HNTs are visible, indicating a good interfacial interaction between PA-11 and HNTs.

TEM micrographs of PA-11 filled with 2, 4, and 6 wt % of HNTs further confirm the SEM observations (Figure 2). Nanotubes are homogeneously dispersed and distributed in the matrix with isolated single nanotubes without any aggregates regardless of the HNT content in the nanocomposites. The high shear extrusion process and the low hydrodynamic interactions on the surface of halloysites favor their compatibility with PA-11, leading to highly dispersed state of HNTs in PA-11 matrix. Further, tubular structures are clearly visible, but their dimension (diameter, <80 nm) is relatively lower than that mentioned in the supplier data sheet. Such changes in nanotubes dimension may be caused primarily by microtoming during the preparation of TEM samples, which enables us to observe some stubs on the TEM images.

Optical Properties

In general, the interfacial refractive index difference between the matrix and the size of dispersed domains governs the optical properties of polymer composites.[36] Depending on the dispersion state of nanofiller, incorporation of nanofiller usually affects the transparency of the polyamides, resulting in an optical clarity loss in the nanocomposites. This is attributed to the fact that nonuniform dispersion of nanofiller tends to aggregate
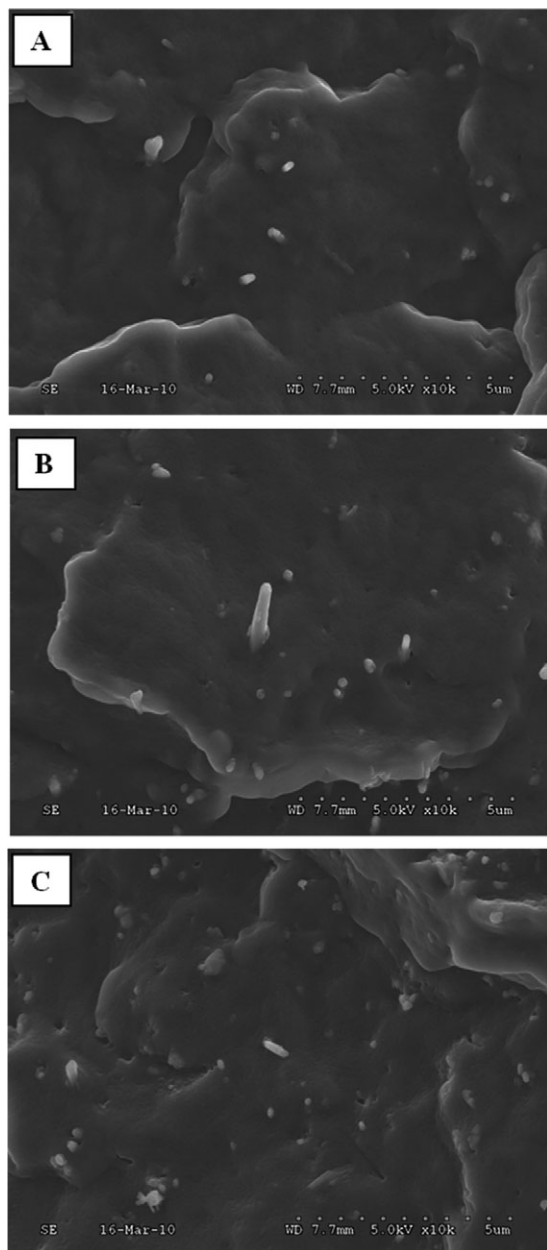
Figure 1. SEM images of PA-11 with (A) 2 wt %, (B) 4 wt %, and (C) 6 wt % HNTs.

As no significant loss of light transmittance can be detected, it is confirmed that PA-11/HNT nanocomposite prepared by melt mixing exhibit uniform nanofiller dispersion in the matrix.
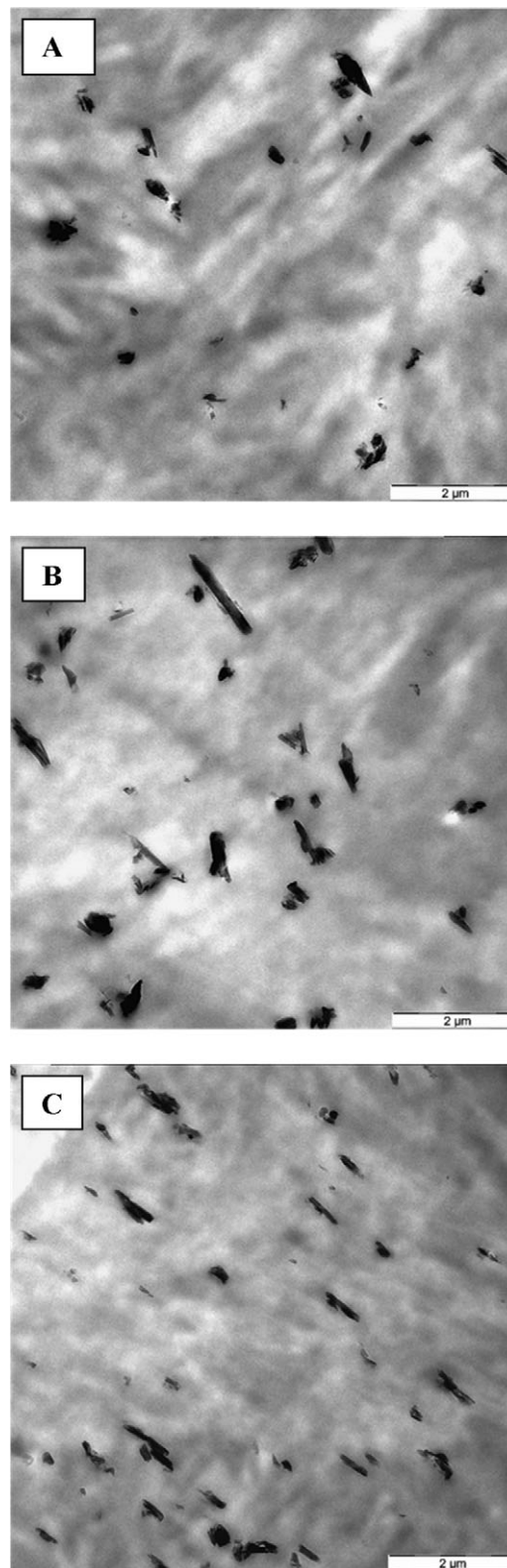

Figure 2. TEM images of PA-11 with (A) 2 wt %, (B) 4 wt %, and (C) 6 wt % HNTs.

into macroscopic size filler, which scatters light and decreases the optical quality of the nanocomposite.[37] Therefore, to retain the optical properties, uniform dispersion of nanofiller should be stressed when preparing the nanocomposites.

Figure 3 shows the variation in UV–visible transmittance (300–800) spectra of PA-11 and PA-11/HNT nanocomposites containing increasing halloysite content. Compared to neat PA-11, the optical properties of the nanocomposites are marginally affected by the presence of the HNTs. For the neat PA-11, the light transmittance at 700 nm is 82% for neat PA-11, and it decreases to 78% upon addition of 6 wt % HNTs (only slight clarity difference is observed for samples with varying HNTs content).
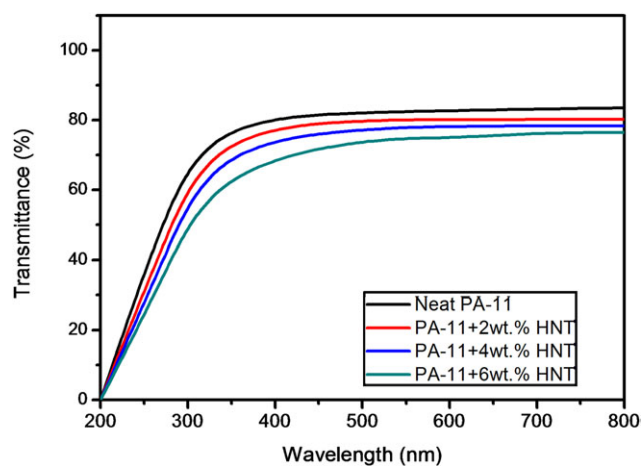
Figure 3. UV–visible transmittance spectra of PA-11/ HNT nanocomposites. [Color figure can be viewed in the online issue, which is available at wileyonlinelibrary.com.]

Table I. Thermal Properties of Nanocomposites with Varying Contents of HNTs

Sample	T_d (°C)	T_m (°C)	T_c (°C)	X_c (%)	T_g (°C)
Neat PA-11	376	189	159	17.2	52
PA-11 + 2 wt % HNT	387	188	163	19.7	56
PA-11 + 4 wt % HNT	405	189	166	21.3	69
PA-11 + 6 wt % HNT	419	190	169	23.2	73

Thermal Stability

The thermal stability of neat PA-11 and PA-11/HNT nanocomposites was investigated using TGA (Figure 4). The thermal decomposition temperature at 5 wt % weight loss (T_d) for all samples was recorded (Table I). No detectable weight changes are observed before 360°C, indicating the absence of any moisture in the sample. The weight loss of the samples after 370°C primarily arises from the loss of decomposition products of PA-11. The T_d of neat PA-11 is 370°C, which is comparable to the values reported in the literature.[35]

The incorporation of HNTs efficiently improves the thermal stability of PA-11 (Figure 4), as the T_d of the nanocomposites gradually increases with growing halloysite content. It is worth noting that T_d of nanocomposites containing 6 wt % nanotubes increases by 32°C. This is higher than the values reported in the literature,[19] where the addition of organoclays led to 15–20°C increase in T_d of the nanocomposite compared to that of neat PA-11. The enhancement in the thermal stability of polyamide
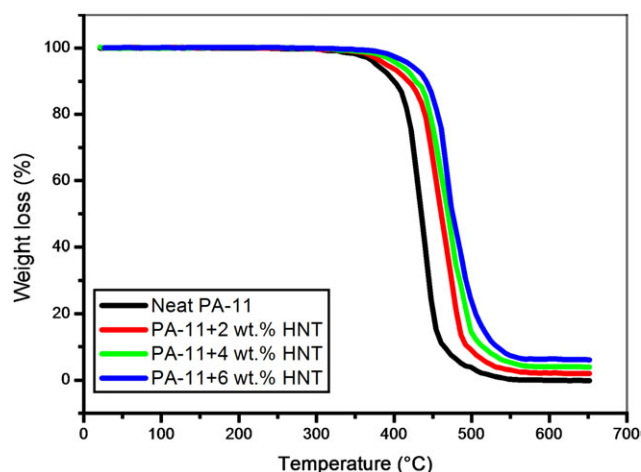
11 (PA11) upon incorporation of HNTs is probably owing to the intrinsic superior thermal stability of HNTs,[38] which promotes the polymer matrix stability via the formation of protecting layers or chars during decomposition process, and also to the excellent thermal conductivity of halloysites. Besides, it was reported that the nanofiller–matrix interfacial interaction also plays an important role in increasing the thermal stability of nanocomposites.[35] In the present case, PA-11/HNT forms good interface as observed by SEM, and one can therefore assume that compatibility between phases markedly reduces the segmented motion of polyamide and thus hinders the diffusion of radicals, oxygen, and decomposition products. In addition, the tubular structure of HNT is another possible reason that increases the T_d of nanocomposites. Du et al.[38] have reported that the degradation products of polypropylene (PP) may be entrapped inside the lumens of HNTs, resulting in effective delay in mass transport and remarkably increased thermal stability of PP/HNT nanocomposites. Similarly, in this case, entrapment of degradation products of PA-11 inside the lumen structure of the HNTs may contribute to the increase in onset decomposition temperature of nanocomposites by a synergy with slow segmental motion and good interfacial quality.[38]

Thermal Behavior

Effect of halloysites' addition on the melting and crystallization behavior of the materials was further investigated using DSC (Figure 5). The crystallization temperature (T_c) and melting temperature (T_m) were measured from the DSC thermograms (Table I).

The thermograms recorded during cooling indicate that T_c slightly increases with growing halloysite content compared to neat PA-11. The increase in crystallization temperature means that the crystallization process is easier in the case of the nanocomposites, indicating a nucleating effect of halloysites in PA-11 matrix. The melting temperature (T_m) remains unaltered with increasing nanotube concentration. However, the intensity of shoulder peak after melting peak increases with increasing filler concentration. The appearance of this shoulder peak is attributed to the melting of preferentially oriented PA-11 macromolecules, such an orientation being explained by the presence of the rigid nanofillers.[21] The degree of crystallinity (X_c) of PA-11 increases with the addition of HNTs. This is consistent with the crystallization behavior of other semi-crystalline polymers in the presence of halloysites, such as PP[28] and PA-6.[29]

Rheological Behavior

The rheological properties of polymer nanocomposites are crucial in gaining insights into the processability and the

Figure 4. TGA of PA-11/HNT nanocomposites. [Color figure can be viewed in the online issue, which is available at wileyonlinelibrary.com.]
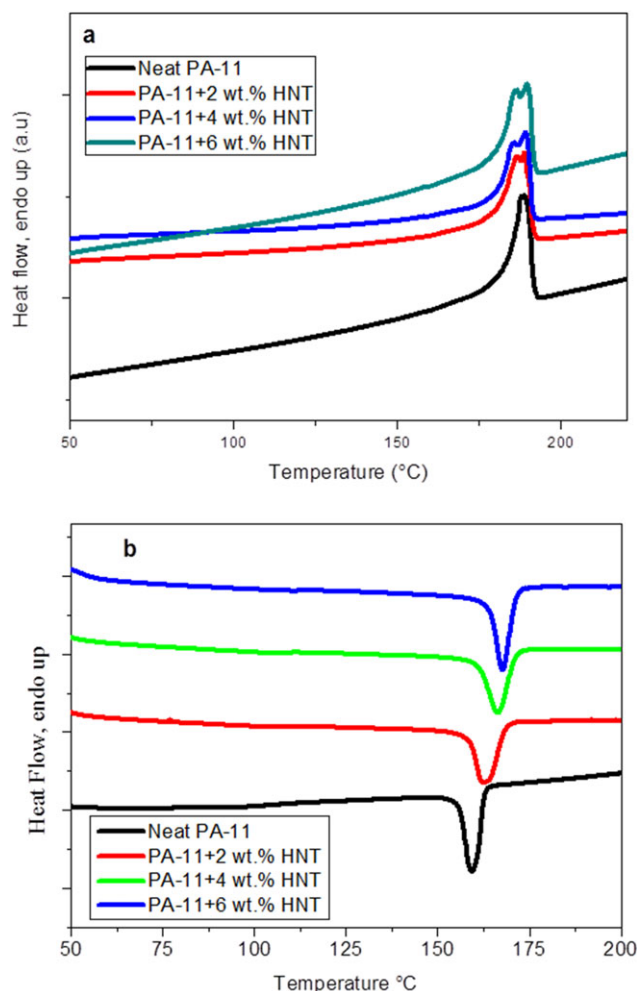
Figure 5. DSC thermograms for the PA-11/HNTs during heating (A) and cooling (B) of nanocomposites at different nanotube contents. [Color figure can be viewed in the online issue, which is available at wileyonlinelibrary.com.]

Viscoelastic Behavior

To further analyze the viscoelastic properties, DMAs were performed on the prepared materials. The variation in the storage modulus in tension (E') and the loss factor (tan δ) with respect to temperature were recorded for neat PA-11 and PA-11/HNT nanocomposites (Figure 7). PA-11/HNT nanocomposite exhibits E' values higher than that of neat PA-11 over the entire temperature range investigated. Furthermore, the E' of the nanocomposite samples increases steadily with increasing halloysite amounts (reaching an increment of + 40% for the nanocomposite containing 6 wt % HNTs compared to neat PA-11), meaning that HNTs act as effective reinforcing fillers. Such a significant improvement in storage modulus of PA-11/HNT nanocomposites is attributed to the reinforcement effect of high-performance HNTs together with interfacial interactions between polyamide and halloysites.

Damping spectra obtained from DMA is also thought to be an effective tool to characterize the interface of filled polymer systems.[39,40] The glass transition temperatures (T_g) may be
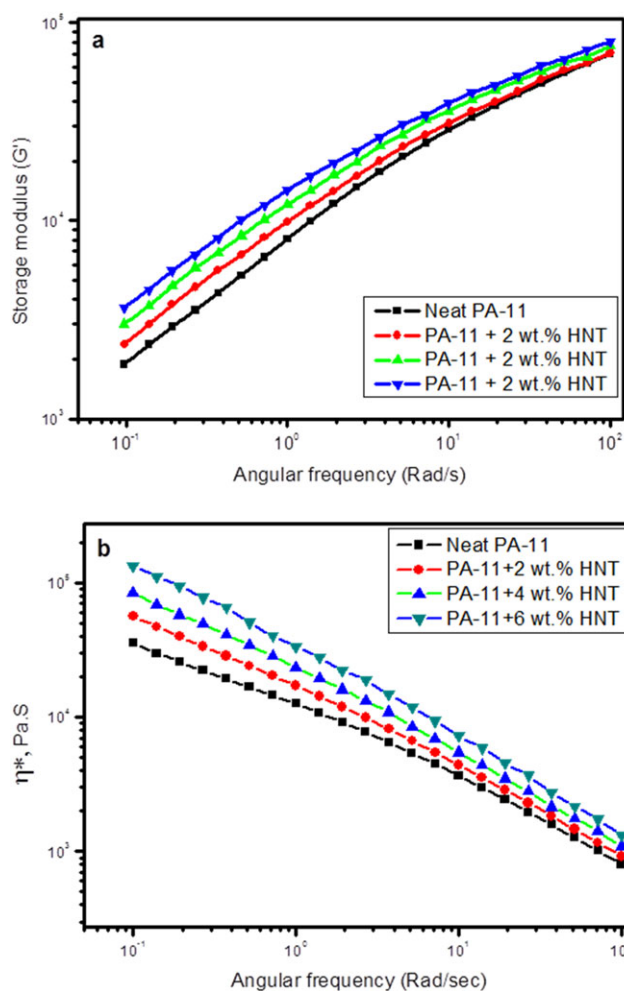

Figure 6. Storage shear modulus (G') (A) and complex viscosity (η^*) (B) of PA-11/HNT nanocomposites with frequency sweep as a function of HNT content at 230°C. [Color figure can be viewed in the online issue, which is available at wileyonlinelibrary.com.]

structure–property relationships of these materials. Rheological characterization is also a well-established method to evaluate the dispersion state of the nanofillers.[8,19] The elastic shear modulus (G') and the complex viscosity (η^*) of neat PA-11 and PA-11/HNT nanocomposites were recorded (Figure 6). The storage modulus of the nanocomposites is higher than that of neat PA-11. Also, it increases when the filler concentration in the matrix grows. The G' increase in the lower frequency range is higher than that noticed at higher frequencies. Thus, at higher frequencies, the rheological behavior of the nanocomposites is dominated by the polymer rather than the nanofillers. The complex viscosity also increases with growing HNT content in the matrix. Such enhanced viscosity of the polymer nanocomposites is usually attributed to the flow restriction of polymer chains in the molten state by the nanoparticles. An increase of the storage modulus (G') and the complex viscosity (η^*) in the low-frequency regime is ascribed to the interfacial interactions between polymer chains and filler surface associated with the homogeneous dispersion of halloysites in the PA-11 matrix.[33]
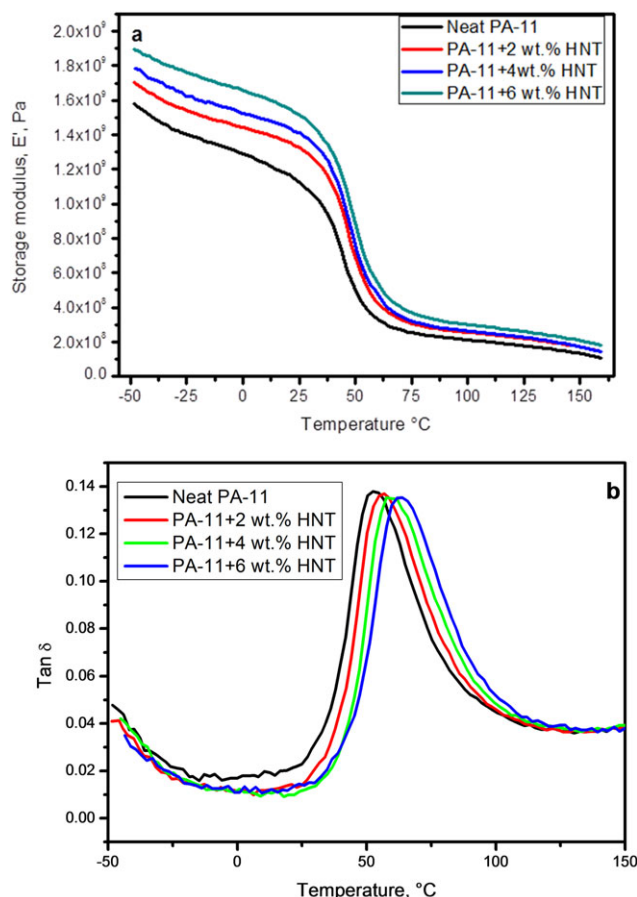
Figure 7. Storage tensile modulus E' (A) and loss factor tan δ (B) of PA-11/HNT nanocomposites with temperature sweep as a function of HNT content. [Color figure can be viewed in the online issue, which is available at wileyonlinelibrary.com.]

extracted in terms of the peak temperature of tan δ versus temperature curves (Table I). The T_g of neat PA-11 (52°C) is lower than the values reported in the literature.[19] Usually, for polya-
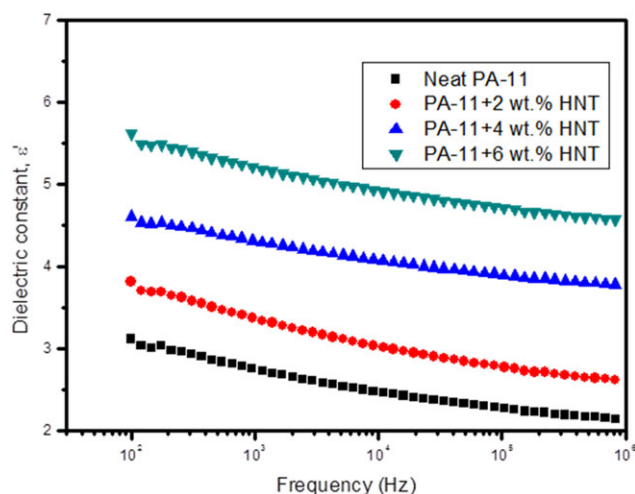

Figure 8. Frequency dependence of real permittivity (ε') for neat PA-11 and PA-11/HNT nanocomposites. [Color figure can be viewed in the online issue, which is available at wileyonlinelibrary.com.]

mides, the T_g depends on the degree of polymerization of the product, and the processing cycle or thermal history that governs the microstructure inside the nanocomposites. Therefore, differences between the processing cycle and the materials' purity used in this study and those adopted in the literature may probably explain the observed difference in the T_g. The glass transition temperature of the PA-11/HNT nanocomposites exhibits a monotonic and linear increase from 56 to 63°C with increasing nanoclay content. Such an increase in the nanocomposites T_g arises from the restricted motion of the segmented PA chains located near the nanotubes surface owing to the hydrogen-bonding interactions between the amine groups of PA-11 chains and the hydroxyl groups on the surface of the nanotubes.[29]

Dielectric Properties

The real permittivity (ε') of the neat PA-11 was compared to those of the PA-11/HNT nanocomposites in the electric field with a frequency range of 102–106 Hz (Figure 8). The real permittivity ε' increases when the HNT concentration grows in the entire studied composition range. This is owing to the polar characteristics of HNTs and thus increases the number of charge carriers in the PA-11 matrix. Also, ε' of all the samples decreases with increasing frequency. This may be ascribed to the fact that the interfacial dipoles do not have enough time to orient themselves in the applied field direction. Therefore, with increase in frequency, the interfacial polarization decreases, resulting in the decrease in dielectric constant.[41] The increase in dielectric constant over all the frequency range, which can be attributed to the homogenous dispersion of halloysites in the PA-11 matrix and the PA-11/HNT compatibility, is consistent with our previous reports on CNT-filled PP nanocomposites.[42]

Mechanical Behavior

The incorporation of HNTs to PA-11 significantly enhances the tensile properties such as modulus, strength, and elongation at break (Table II). The tensile elastic modulus of the neat PA-11 is 1.22 GPa, which is consistent with the values reported by Stoclet et al.[22] Increasing the HNT content in PA-11 leads to a continuous increase of modulus. However, the relative increment obtained with 2 wt % HNT contents is more remarkable compared to that noticed with higher HNT contents. Adding 2 wt % HNTs into PA-11 results in a + 32% increase in modulus compared to neat PA-11, whereas incorporation of 6 wt % HNTs induces an increase limited to + 57% only, meaning that

Table II. Tensile Properties of Nanocomposites as a Function of HNT Content

Sample	Young's Modulus (MPa)	Tensile strength (MPa)	Elongation at break (%)
Neat PA-11	1220 ± 12	43.7 ± 2.5	254 ± 7
PA-11 + 2 wt % HNT	1616 ± 14	48.8 ± 1.8	251 ± 6
PA-11 + 4 wt % HNT	1781 ± 13	52.5 ± 2.1	245 ± 6
PA-11 + 6 wt % HNT	1915 ± 15	54.2 ± 2.5	235 ± 8

Table III. Percentage Variation in Tensile Properties of Nanocomposites Containing MWNT, MMT and HNT Nanofillers (Compared with Neat PA-11 Matrix)

Tensile properties	Property variation in percentage (compared with neat PA-11 matrix) of nanocomposites containing 4 wt % fillers		
	MWNT(44) (%)	MMT-clays(43) (%)	HNT (%)*
Modulus	+32.0	+56.9	+46.7
Strength	+28.0	+18.4	+20.0
Elongation at break	−90.5	−34.0	−3.5

only an extra + 25% increase can be achieved by incorporating the additional 4 wt % HNTs.

The effects of HNT on tensile strength and elongation were also investigated (Table II). The addition of HNT obviously enhances the strength of PA-11. Again, tensile strength increases significantly at lower HNTs content (2 and 4 wt %) and then relatively less at higher loading (6 wt %). Interestingly, all the nanocomposites exhibit an increase in tensile modulus and strength without any significant loss of ductility. No depletion in the elongation at break for HNT-filled PA-11 matrix is an unusual case and is owing to the strong strain hardening of the PA-11 matrix imparted by the rigid HNTs.[29] The enhancement of the mechanical properties of the composites relies on many factors such as morphology of the polymeric matrix in terms of filler dispersion and crystallinity. SEM and TEM studies revealed a good dispersion of the nanotubes in the polymeric matrix with a strong interfacial adhesion between the phases, leading to a high level of load transfer between the matrix and the nanotubes. Increase in tensile properties is also owing to the increase in degree of crystallinity induced by the addition of halloysites as observed in DSC analysis. Similar results were reported for nanocomposites based on PA-6 filled with HNTs.[29]

Comparison of PA-11 Nanocomposites Based on Various Nanofillers

Halloysite nanotubes have become interesting nanofillers for polymers in recent past. HNTs are intrinsically strong naturally available material with tubular structure and, depending on the application field, they can replace layered silicates and CNTs. Therefore, it is felt worth to compare the reinforcement efficiency of halloysites with other nanofillers such as layered silicates such as MMTs[43] and CNTs (multiwalled nanotubes, MWNTs)[44] melt processed with polyamide-11 under similar conditions. Table III lists the percentage variations in tensile properties of melt-processed PA-11 nanocomposites containing 4 wt % of MWNTs, MMTs, and HNTs with respect to neat PA-11 matrix. MMTs showed a higher increase in tensile modulus than MWNTs and HNTs. MWNTs exhibit better tensile strength when compared to other nanofillers. Nonetheless, the performance of HNTs is very interesting as they display a balanced increase in modulus and strength without sacrificing the ductility. Although the elongation at break decreases drastically by

−90.5% for CNTs and by about −34% for MMT, it remains almost unaltered for halloysites (−3.5%). These results clearly indicate that HNTs provide the best reinforcement potential compared with CNTs and MMTs. This is owing to the fact that entangled CNTs aggregates are difficult to disperse with conventional polymer-processing methods. In the case of MMTs, achievement of well-exfoliated morphology still remains a technical challenge. Therefore, the presence of clay tactoids and agglomerates usually reduces the mechanical properties of the resulting nanocomposites. On the contrary, HNTs are less prone to form agglomerates owing to the low hydroxyl group density on their surface and therefore halloysites may not require any pretreatment process, as required by MMTs. Additionally, cost-effectiveness, natural availability, and biocompatibility of HNTs make these nanotubes an attractive filler in the preparation of high-potential advanced materials in polymer nanocomposites field.

CONCLUSIONS

Bio-based PA11/natural HNTs nanocomposites with varying nanotube concentrations were prepared by melt extrusion using a masterbatch dilution process. The materials were analyzed for microstructural changes, transparency, thermal stability, rheological behavior, dielectric, and tensile properties.

The HNTs appear to be uniformly dispersed in PA-11 matrix in the studied composition range as shown by SEM and TEM observations and confirmed by UV–visible spectrophotometry, the optical properties of the PA-11/HNT nanocomposites being only marginally affected by the presence of the HNTs. As expected, PA-11/HNT nanocomposites exhibit a more pronounced solid-like and stronger shear thinning behavior than neat PA-11, which is more prominent at higher HNT contents. Interestingly, good halloysite dispersion in PA-11 matrix increases the tensile strength and Young modulus of PA-11 without sacrificing the ductility. Highly dispersed nanotubes also significantly improve the thermal stability of the nanocomposites. Inclusion of HNTS in PA-11 matrix also brings favorable changes in the dielectric characteristics of PA-11 (increase in permittivity partially ascribed to the interfacial polarization between PA-11 and HNTs). Additionally, as HNTs added in the PA-11 matrix act as nucleating agents, crystallization temperature and degree of crystallinity of the nanocomposites tend to increase with growing nanotubes loading. The glass transition temperature follows similar trend, whereas the melting temperature is only marginally affected by the presence of nanotubes.

Therefore, combining bio-based polyamide-11 and naturally available HNTs makes sense in view of designing novel green nanocomposite materials with multifunctional properties for specific applications. Detailed investigations on the influence of HNTs on crystalline morphology and deformation behavior of nylon 11 are still in progress.

REFERENCES

1. Gupta, B.;Lacrampe, M.-F.; Krawczak, P. *Polym. Polym. Compos.* **2006**, *14*, 13.

2. Prashantha, K.; Soulestin, J.; Lacrampe, M.-F.; Krawczak, P. *Polym. Polym. Compos.* **2009**, *17*, 205.

3. Naveau, E.; Dominkovics, Z.; Detrembleur, C.; Jérôme, C.; Hári, J.; Renner, K.; Alexandre, M.; Pukánszky, B. *Eur. Polym. J.* **2011**, *47*, 5.

4. Soulestin, J.; Rashmi, B. J.; Bourbigot, S.; Lacrampe, M.-F.; Krawczak, P. *Macromol. Mater. Eng.* **2012**, *297*, 444.

5. Touchaleaume, F.; Soulestin, J.; Sclavons, M.; Devaux, J.; Lacrampe, M. F.; Krawczak, P. *Polym. Degrad. Stab.* **2011**, *96*, 1890.

6. Mishra, S.; Sonawane, S. S.; Shimpi, N. G. *Appl. Clay Sci.* **2009**, *46*, 222.

7. Yang, J.-L.; Zhang, Z.; Zhang, H. *Comp. Sci. Tech.* **2005**, *65*, 2374.

8. Ou, B.; Li, D.; Liu, Y. *Comp. Sci. Tech.* **2009**, *69*, 421.

9. Li, J.; Tong, L.; Fang, Z.; Gu, A.; Xu, Z. *Polym. Degrad. Stab.* **2006**, *91*, 2046.

10. Logakis, E.; Pandis, Ch.; Peoglos, V.; Pissis, P.; Pionteck, J.; Pötschke, P.; Mičušík, M.; Omastová, M. *Polymer* **2009**, *50*, 5103.

11. Brosse, A. C.; Tencé-Girault, S.; Piccione, P. M.; Leibler, L. *Polymer* **2008**, *49*, 4680.

12. Bulter, S.; Kim, G.; Koo, J. H.; Londa, M.; Wagner, A.Flame retardant polyamide 11-halloysite nanotube nanocomposites: Mechanical, thermal, and flammability characterization. Proc. SAMPE 2011 ISTC, Fort Worth, TX, October 17–20, **2011**.

13. Rhee, S.; White, J. L. *J. Polym. Sci. Part B: Polym. Phys.* **2002**, *40*, 2624.

14. Kremmer, A.; Neumann, W.; Gerhard-Multhaupt, R.; Guy, I. L. *IEEE Trans. Dielectr. Electr. Insul.* **2004**, *11*, 271.

15. Chen, P. K.; Newman, B. A.; Scheinbeim, J. I.; Pae, K. D. *J. Mater. Sci.* **1985**, *20*, 1753.

16. Rhee, S.; White, J. L. *J. Polym. Sci. Part B: Polym. Phys.* **2002**, *40*, 1189.

17. Rhee, S.; White, J. L. *Polym. Eng. Sci.* **2002**, *42*, 134.

18. Newman, B. A., Pae, K. D., Scheinbeim, J. I. (United States Patent and Trademark Office) U.S. Patent 4,486,683., **1984**.

19. Liu, T.; Lim, K. P.; Tjiu, W. C.; Pramoda, K. P.; Chen, Z.-K. *Polymer* **2003**, *44*, 3529.

20. He, X.; Yang, J.; Zhu, L.; Wang, B.; Sun, G.; Lv, P.; Phang, I. Y.; Liu, T. *J. Appl. Polym. Sci.* **2006**, *102*, 542.

21. Mago, G.; Kalyon, D. M.; Fisher, F. T. *J. Polym. Sci. Part B: Polym. Phys.* **2011**, *49*, 1311.

22. Stoclet, G.; Sclavons, M.; Devaux, J. *J. Appl. Polym. Sci.* **2013**, *127*, 4809.

23. Du, M.; Guo, B.; Jia, J. *Polym. Int.,* **2010**, *59*, 574.

24. Frost, R. L.; Shurvell, H. F. *Clay Miner.* **1997**, *45*, 68.

25. Vergaro, V.; Abdullayev, E.; Lvov, Y. M.; Zeitoun, A.; Cingolani, R.; Rinaldi, R.; Leporatti, S. *Biomacromolecules* **2010**, *11*, 820.

26. Price, R. R.; Gaber, B. P.; Lvov, Y. *J. Microencaps.* **2001**, *18*, 713.

27. Shchukin, D.; Price, R.; Sukhorukov, G.; Lvov, Y. *Small,* **2005**, *1*, 510.

28. Prashantha, K.; Lacrampe, M.-F.; Krawczak.P. *Express Polym. Lett.* **2011**, *5*, 295.

29. Prashantha, K.; Schmitt, H.; Lacrampe, M.-F.; Krawczak, P. *Compos. Sci. Tech.* **2011**, *71*, 1859.

30. Schmitt, H.; Prashantha, K.; Schmitt, H.; Soulestin, J.; Lacrampe, M.-F.; Krawczak, P. *Carbohydr. Polym.* **2012**, *89*, 920.

31. Hedicke-Höchstötter, H.; Lim, G. T.; Altstädt, V. *Compos. Sci. Tech.* **2009**, *69*, 330.

32. Liu, M.; Guo, B.; Du, M.; Chen, F.; Jia, D. *Polymer* **2009**, *50*, 3022.

33. Lecouvet, B.; Sclavons, M.; Bourbigot, S.; Devaux, J.; Bailly, C. *Polymer* **2011**, *52*, 4284.

34. Prashantha, K.; Soulestin, J.; Lacrampe, M.-F.; Krawczak, P.; Dupin, G.; Claes, M. *Compos. Sci. Tech.* **2009**, *69*, 1756.

35. Huang, S.; Wang, M.; Liu, T.; Zhang, W.-D.; Tjiu, W. C.; He, C.; Lu, X. *Polym. Eng. Sci.* **2009**, *49*, 1063.

36. Lai, S.-M.; Chen, C.-M. *Eur. Polym. J.* **2007**, *43*, 2254.

37. Faghihi, K.; Shabanian, M. *High Temp. Mater. Process.* **2011**, *1*, 77.

38. Du, M., Guo, B.; Jia, D. *Eur. Polym. J.* **2006**, *42*, 1362.

39. Burnside, S. D.; Giannelis, E. P. *J. Polym. Sci. Part B: Polym. Phys.* **2000**, *38*, 1595.

40. Rao, Y. Q.; Pochan, J. M. *Macromolecules* **2007**, *40*, 290.

41. Cavallaro, G.; Ines, D.; Lazzara, G.; Milioto, S. *J. Phys. Chem. C.* **2011**, *115*, 20491.

42. Prashantha, K.; Soulestin, J.; Lacrampe, M.-F.; Krawczak, P.; Dupin, G.; Claes, M.; Tewari, A. *Polym. Polym. Compos.* **2010**, *18*, 489.

43. Fornes, T. D.; Paul, D. R. *Macromolecules* **2004**, *37*, 7698.

44. Lao, S. C.; Koo, J. H.; Yong, W.; Lam, C.; Zhou, J.; Moon, T.; Piccione, P. M.; Wissler, G.; Pilato, L.; Luo, Z. P.Polyamide 11-Carbon nanotubes nanocomposites: preliminary investigation. Proc. Int. SAMPE 2011 ISSE, Long Beach, CA, USA, May 23–26, **2011**.